journal

J. Am. Ceram. Soc., 91 [10] 3240–3244 (2008)
DOI: 10.1111/j.1551-2916.2008.02536.x

Effects of SRO Buffer Layer on Multiferroic $BiFeO_3$ Thin Films

R. Y. Zheng, C. H. Sim, and J. Wang†

Department of Materials Science and Engineering, Faculty of Engineering, National University of Singapore, Singapore 117574, Singapore

S. Ramakrishna

Division of Bioengineering, Faculty of Engineering, National University of Singapore, Singapore 117574, Singapore

Crystallization, surface morphology, and electrical behavior of $BiFeO_3$ thin films are improved by $SrRuO_3$ (SRO) buffer layer with optimized grain size. Large-grained SRO buffer layer promotes the growth of dense multiferroic $BiFeO_3$ (BFO) thin films and reduces structural defects. Phase identification by using X-ray diffraction and surface morphology studies by using scanning electron microscopy show that the large-grained SRO buffer layer formed by sputtering thicker SRO films promotes the formation of the perovskite phase as well as the crystallinity. These BFO films have also shown reduced leakage current, as suggested by the weaker frequency dependence of the ferroelectric hysteresis loops as compared with the BFO films deposited on smaller-grained SRO buffer layer. Investigation into the dielectric properties and fatigue endurance reveals that the structural defects of the BFO thin film have also been reduced by employing the larger-grained SRO buffer layer.

I. Introduction

An increasing interest has recently been devoted to the study of mutiferroic materials due to their attractive multifunctional properties. The magnetoelectric effect, which allows coupling between the ferroelectric and ferromagnetic behavior, make this class of materials a very attractive candidate for several technological applications. Lately, a surge in interest of multiferroic $BiFeO_3$ (BFO) was triggered by the report of a gigantic polarization of $\sim 90\ \mu C/cm^2$ by Wang *et al.*[1] Bulk BFO exhibits the co-existence of ferroelectric and antiferromagnetic behavior, while thin-film BFO shows both ferroelectric and with weak ferromagnetic properties.[1–5] Intense investigation has been made into this class of materials, which promise immediate applications in the ferroelectric random access memories.[6] Indeed, the desirable electrical properties and the potential applications of BFO make it a strong candidate to replace $Pb(Zr,Ti)O_3$ (PZT), which has been the main material for various ferroelectric/piezoelectric devices.

Although BFO thin films possess excellent ferroelectric properties required for memory device applications, a drawback that limits their applications is their high leakage current, which is believed to be related to the presence of oxygen vacancies and variable Fe oxidation states (i.e., Fe^{2+} or Fe^{3+}).[7–9] Although the exact mechanism responsible for the high leakage current in BFO is still controversial, approaches such as adding dopants into the BFO structure,[2,10,11] forming solid solution of BFO with other ABO_3, such as $PbTiO_3$,[9,11] and depositing BFO on different types of substrates[3,12,13] have been taken to reduce the leakage current in these materials. Despite the type of substrate used for thin film deposition has been widely reported to be crucial in determining the performance of the resultant thin film, no study has been carried out so far to optimize the substrate condition and completely solve the leakage problem in BFO thin films. In this paper, we report the effects of the morphology of $SrRuO_3$ (SRO) buffer layer on the ferroelectric and dielectric properties of the BFO films deposited upon. The grain size of the SRO buffer layer is varied by using different sputtering time. A close comparison is made between the BFO films rf sputtered on SRO buffer layers of various grain sizes. Our study reveals that the crystallization of the BFO perovskite phase, surface morphology and electrical properties are all strongly affected by the grain size of the bottom SRO buffer layer.

II. Experimental Procedure

In this study, SRO buffer layers of ~ 40 and ~ 80 nm in thickness were deposited on $Pt/TiO_2/SiO_2/Si$ substrates by rf sputtering from a 2 in. strontium ruthenium oxide ceramic target (SCI Eng. Mat.) at a substrate annealing temperature of 600°C for 15 and 30 min (namely, SRO 15-min and SRO 30-min buffer layers), respectively. A BFO target with 10 wt% excess Bi was prepared from Bi_2O_3 and Fe_2O_3 via solid-state reaction and sintered at 850°C. BFO films of ~ 220 nm were then subsequently deposited on top of the SRO 15- or 30-min buffer layers by rf sputtering the BFO ceramic target. The BFO films were deposited on either the SRO 15-min or SRO 30-min buffer layer under identical sputtering conditions, but at two different substrate temperatures of 650° and 680°C, respectively.

The phases present in the BFO thin films were analyzed by using X-ray diffraction (Bruker D8 Advanced XRD, Bruker AXS Inc., Madison, WI, Cu$K\alpha$). Scanning electron microscopy (SEM, Philips, XL 30, Hillsboro, OR) was used to study the surface morphology and the cross section of the thin films. Film thickness was measured using Alpha-Step Profilometer (Alpha-step 500, Tencor, San Jose, CA). Their ferroelectric and fatigue properties were studied by using the Radiant precise workstation (Radiant Technologies, Medina, NY). An impedance analyzer (Solartron 1261, Farnborough, UK) was used to measure the dielectric properties, and the leakage current behaviors were characterized by using a Keithley meter (Keithley 6430, Cleveland, OH). Circular Au electrodes of diameter 0.2 mm were sputtered on the BFO film surface using a shadow mask, in order to investigate the electrical properties of the thin films. Magnetic properties of the thin films were characterized using Superconducting Quantum Interference Devices (SQUID, MPMS, XL-5AC, San Diego, CA).

III. Results and Discussions

A dense and continuous layer structure was revealed, by SEM cross-sectional examination, for the BFO and SRO buffer layer

D. Viehland—contributing editor

Manuscript No. 24192. Received January 7, 2008; approved May 6, 2008.
This work was supported by the Science and Engineering Research Council – A*Star, Singapore, under Grant No. 052 101 0047.
†Author to whom correspondence should be addressed. e-mail: msewangj@nus.edu.sg

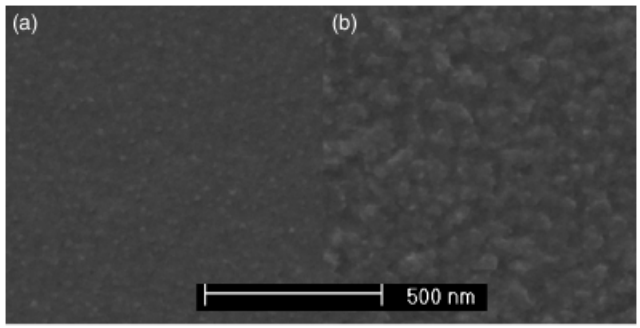

Fig. 1. Scanning electron microscopy images of the SRO buffer layers deposited by rf sputtering on $Pt/TiO_2/SiO_2/Si$ substrates for: (a) 15 min and (b) 30 min, respectively.

deposited on $Pt/TiO_2/SiO_2/Si$ substrates for the samples prepared by using both sputtering times (15 and 30 min). Thicknesses of the SRO layers were determined by Alpha-Step Profilometer to be 86.0 ($\pm$6.65) nm for the SRO film sputtered for 30 min and 44.5 ($\pm$4.46) nm for the SRO film sputtered for 15 min. The surface morphologies of the SRO buffer layers are shown in Fig. 1, which indicate that the films deposited are dense and crack-free. However, larger grains were observed for the SRO buffer layer deposited for 30 min (Fig. 1(b)), as compared with that of the film deposited for 15 min (Fig. 1(a)). The average grain size of the SRO film sputtered for 15 min is 60.4 nm while that of the SRO film sputtered for 30 min is 94.5 nm. Thus a significant increase in grain size (56.4%) was observed in the latter as compared with the former. Surface morphology analysis of the SRO buffer layers by using AFM reveals that mean-square-root surface roughness of the SRO layer sputtered for 30 min was 6.78 nm while that of the SRO layer sputtered for 15 min was only 2.47 nm. Hence, it can be concluded that a longer sputtering and substrate annealing time resulted in larger SRO grains and a rougher film surface.

The BFO films deposited on the SRO buffer layers of two different thicknesses were subsequently studied. They have similar thicknesses of 224.1 ($\pm$55.8) nm as the same sputtering conditions and durations were used. Examination by using SEM show that the BFO films have a distinct cross-sectional interface between the different layers, indicating that the individual SRO and BFO layers were well deposited. Figure 2 shows the XRD diffraction patterns of the BFO films deposited on the SRO 15-min and SRO 30-min buffer layers at 650° and 680°C, respectively. They were identified to be well-crystallized BFO for all these films. No secondary phases were found. They show that the SRO buffer layers did not induce any preferred orientation growth of the BFO thin films. By using the same XRD conditions, the relative crystallinity of the BFO films were studied by comparing their relative peak intensities. Calculation of the (110) peak intensity revealed that the peak intensity of BFO 680°C/SRO 30 min was 41% higher than that of BFO 650°C/

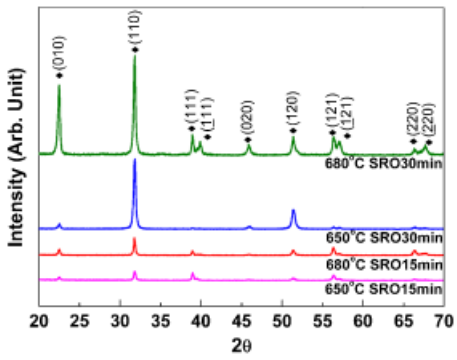

Fig. 2. X-ray diffraction patterns for the BFO thin films deposited on the $SrRuO_3$ (SRO) buffer layers of small grains (SRO 15 min) and large grains (SRO 30 min), and grown at 650° and 680°C, respectively.

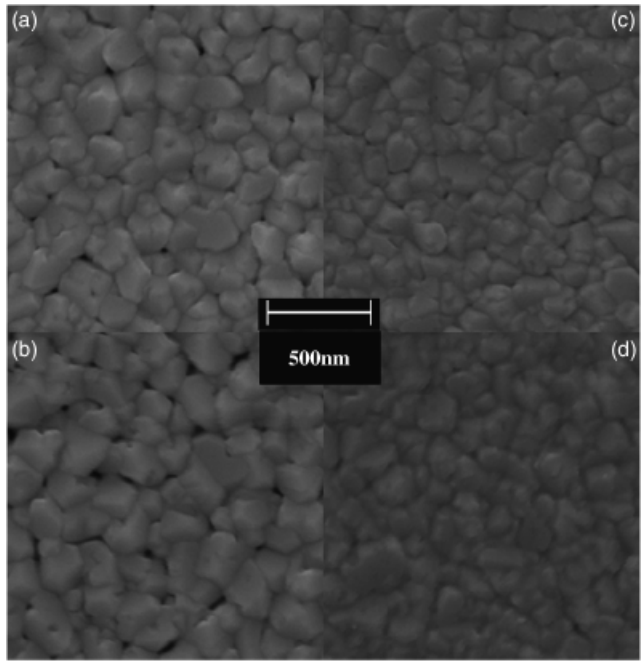

Fig. 3. Scanning electron microscopy images of the BFO thin films rf sputtered on $SrRuO_3$ (SRO) buffer layers of small grains (SRO 15 min) at (a) 650°C and (b) 680°C, and large grains (SRO 30 min) at (c) 650°C and (d) 680°C, respectively.

SRO 30 min, while BFO 680°C/SRO 15 min was 102% higher than that of BFO 650°C/SRO 15 min. The higher XRD peak intensities observed for the BFO films annealed at 680°C as compared with those at 650°C indicate that the crystallinity of BFO films were promoted at a higher annealing temperature. It was also observed that the BFO crystallinity could also depend on the type of the buffer layers. The (110) peak intensity of the BFO 680°C/SRO 30-min film was calculated to be 467% higher than that of the BFO 680°C/SRO 15-min film; the (110) peak intensity of the BFO 650°C/SRO 30 min was calculated to be 708% higher than that of the BFO 650°C/SRO 15-min film. As discussed earlier, the SRO 30-min buffer layer exhibits larger grain sizes. Hence it is apparent that the coarse SRO grains have effectively promoted the growth of the BFO thin film, as shown by the significantly higher peak intensity of the BFO/SRO 30-min films as compared with the BFO/SRO 15-min films. The crystallinity of the BFO phase deposited on top of the SRO buffer layer can thus be promoted by either a higher annealing temperature or by depositing BFO thin films on a larger-grained SRO buffer layer.

Surface morphologies of the BFO films shown in Fig. 3 reveal that the BFO films deposited on SRO 30 min were denser for both the annealing temperatures of 650° and 680°C, while the pair of BFO/SRO 15-min films were obviously more porous. The average grain sizes of the BFO films annealed at 650° and 680°C, deposited on SRO 15 min, are 179 and 197 nm, respectively, while those of the BFO films deposited on SRO 30-min films are 152 and 153 nm. Therefore, the SRO 30-min buffered substrate with larger grains was effective in promoting the growth of a denser BFO film with smaller grains.

Figures 4(a) and (b) plot the polarization–electric field (P–E) hysteresis loops of the BFO films, deposited on the two different SRO buffer layers. One can see that the two BFO thin films deposited on SRO 15 min show a higher "apparent" double remanent polarization ($2P_r$), as compared with those on SRO 30 min. However, both of the BFO/SRO 15-min films demonstrate a high leakage from their P–E loops e.g., the rounded drop-down tips in the hysteresis loops, especially for the BFO 680°C/SRO 15-min film. These experimental observations indicate that leakage and space charge contribute to the polarization response in the BFO/SRO 15-min thin films. In contrast,

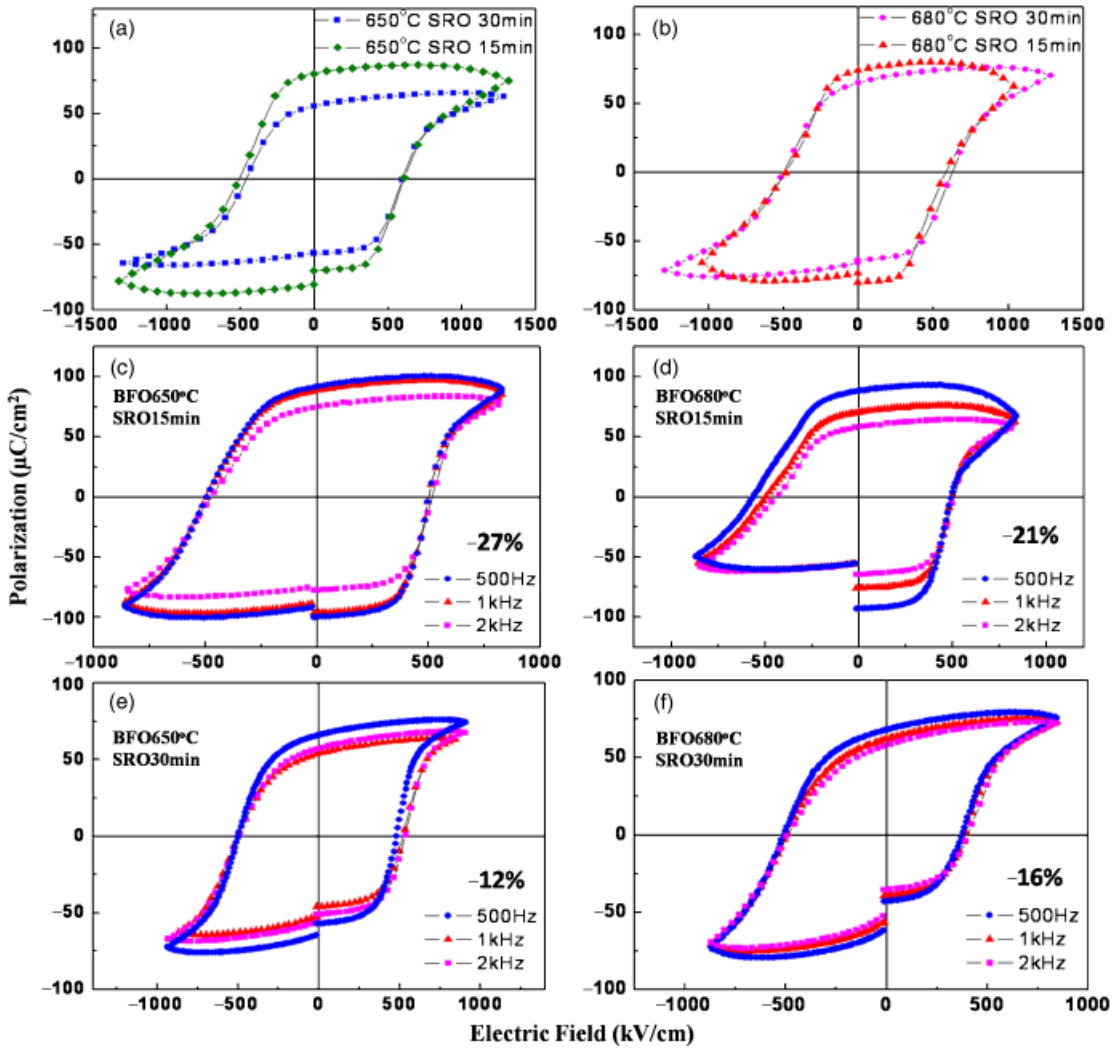

Fig. 4. Hysteresis loops of the four BFO films deposited on $SrRuO_3$ (SRO) buffer layers of small grains (SRO 15 min) and large grains (SRO 30 min), at (a) 650°C and (b) 680°C, respectively. Frequency series of *P–E* hysteresis loops for the four BFO films rf sputtered on SRO buffer layers of small grains (SRO 15 min) at (c) 650°C and (d) 680°C and large grains (SRO 30 min) at (e) 650°C and (f) 680°C. Measurements were conducted at three different frequencies of 500 Hz, 1 kHz, and 2 kHz.

the BFO films deposited at 650° and 680°C on SRO 30-min buffer layer display well-established square-shaped *P–E* loops with giant polarizations ($2P_r$) of 112.5 and 130.0 μC/cm^2, and coercive fields ($2E_c$) of 1045.5 and 1125.1 kV/cm, respectively.

To verify the extent of space charge effect, hysteresis loop measurements were carried out at different frequencies, in order to study the intrinsic ferroelectric properties of the BFO films. Figure 4(c)–(f) plots the frequency dependence of *P–E* hysteresis loops for the four BFO films. These measurements were conducted at three different frequencies of 500 Hz, 1, and 2 kHz. All four films exhibit a degree of frequency dependence, and a lower $2P_r$ is measured at higher frequency. In particular, one can note that much stronger frequency dependence is exhibited by the pair of BFO/SRO 15-min films, showing a significant decrease of $2P_r$ as frequency increases from 500 Hz to 2 kHz. For the BFO/SRO 15-min films thermally annealed at 650° and 680°C, a decrease in polarization of −27 and −21% at 2 kHz was observed, respectively, as compared with those measured at 500 Hz. In contrast, the BFO/SRO 30-min films thermally annealed at 650° and 680°C demonstrate a weaker frequency dependency, and the polarization decreases only −12 and −16%, respectively. Hence, it is concluded that the space charge in the BFO/SRO 15-min samples contributes more toward the polarization response. As aforementioned, the BFO thin film deposited on SRO 15-min buffer layer shows a lower crystallinity, poor porosity, and rougher film surface textures, all of which can apparently lead to a large leakage current and serious space charge effect. It should be noted that the BFO 650°C/SRO 30-min film exhibits very well-established square-shaped hysteresis loops for all three frequencies used in the present work. As shown in Fig. 4(d), even at the frequency as high as 2 kHz, the film still exhibited a high $2P_r$ of 108.2 μC/cm^2.

Figure 5 shows the fatigue behaviors of the four BFO thin films drove by triangular bipolar pulses of 200 kHz and 16 V. A polarization degradation of ~17 and ~31% was measured for the BFO/SRO 30-min films annealed at 650° and 680°C, respectively, after 10^{10} switching cycles, indicating a much better fatigue resistance than conventional PZT films.[14] Interestingly, the switchable polarizations of the BFO/SRO 15-min films were enhanced at the early stage of the fatigue test, followed by polarization degradations after ~10^7 and ~10^9 cycles for the samples annealed at 650° and 680°C, respectively. Similar exotic fatigue behaviors have been reported for PZT thin films.[15] Such fatigue behavior has been attributed to the defects in the thin PZT thin films. The apparent polarization enhancement during fatigue measurements supports what was discussed above that the BFO/SRO 15-min films exhibited more structural defects.

The observed difference in structure of the BFO films also has a dramatic effect on their dielectric properties. The relative permittivity of the BFO/SRO 15-min films decreases drastically with increasing frequency from 1 to 10^5 Hz. The BFO/SRO 15-min films that were thermally annealed at 650° and 680°C

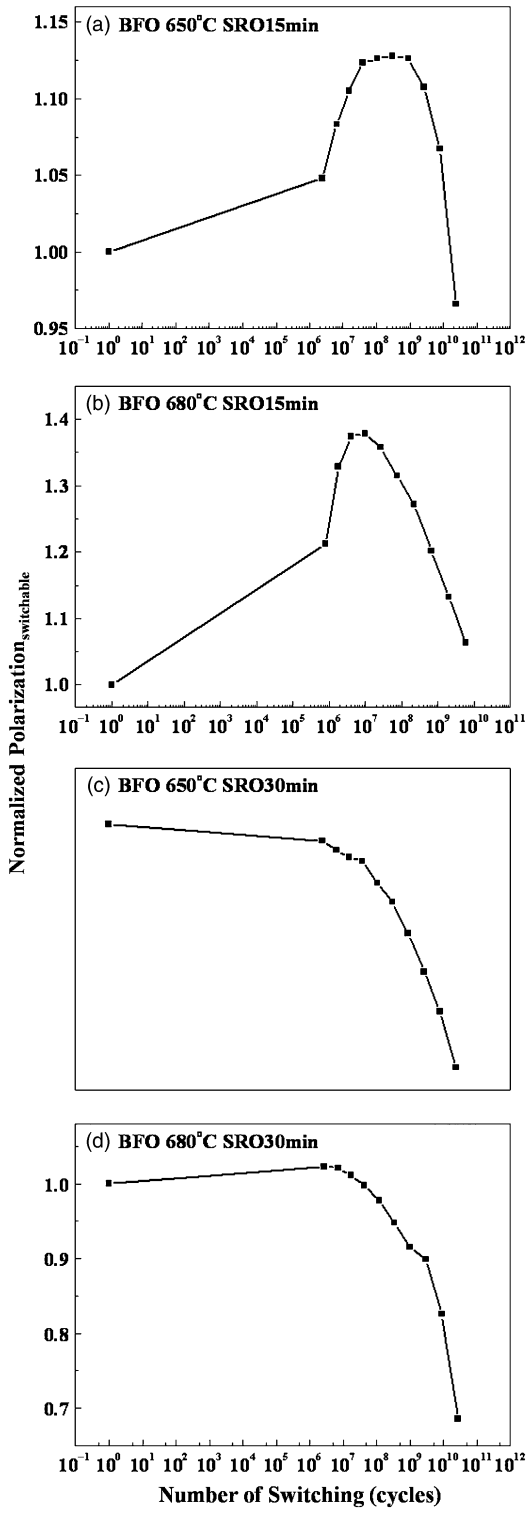

Fig. 5. Fatigue behavior of the four BFO films rf sputtered on $SrRuO_3$ (SRO) buffer layers of small grains (SRO 15 min) at (a) 650°C and (b) 680°C and large grains (SRO 30 min) at (c) 650°C and (d) 680°C, respectively, driven by triangular bipolar pulses of 16 V and 200 kHz.

both exhibited tangent loss peaks signifying dielectric relaxation at around 10^3 and 10^4 Hz, respectively. Such tangent loss characteristics are consistent with their respective relative permittivity plots, where a sudden decrease in the relative permittivity at the two characteristic frequencies was observed. The dielectric behaviors of BFO/SRO 15-min films at low frequencies confirm the conclusion made above concerning the contribution of space charges towards the polarization hysteretic properties of the thin films. The space charges leading to the dielectric relaxation

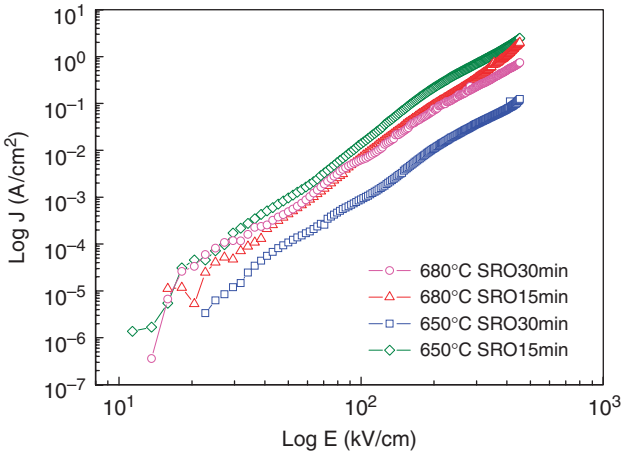

Fig. 6. Leakage current density as a function of applied electrical field for the four BFO films deposited on $SrRuO_3$ (SRO) buffer layers of small grains (SRO 15 min) and large grains (SRO 30 min), thermally annealed at 650° and 680°C, respectively.

shown above are due to the structural defects such as oxygen vacancies. It is well known that defect-induced dielectric relaxations are directly related to the defect concentration.[9,16] Furthermore, significantly higher tangent loss values were measured with the BFO/SRO 15-min films as compared with those on the corresponding BFO/SRO 30-min films, which again indicate a higher space charge concentration in the BFO/SRO 15-min films. This gives rise to a broad hump in the dielectric loss spectrum in the BFO/SRO 15-min films.[17]

Figure 6 shows the leakage current behavior for the four BFO films. The BFO films deposited on SRO 30-min buffer layers at 650° and 680°C, respectively, exhibit a lower leakage current as compared with the other two, consistent with their *P–E* hysteresis loops and dielectric measurements shown above. It can be seen that the BFO 650°C/SRO 30-min film exhibits the lowest leakage current, which is nearly one order of magnitude lower than the other three. These results confirm that the BFO films deposited on SRO 30-min buffer layer exhibit a denser and well-crystallized BFO structure, and therefore a lower leakage. The linear log J versus log E curves of all the four BFO thin films indicate a power law relation, $J \propto E^{\alpha}$. The linearity of the slopes, α, of the log J–log E plot, is characteristic of the space charge limited conduction (SCLC), which corresponds to the shallow trap square law: $J\mu k\varepsilon_o\theta L^3$, where μ is the mobility of the charge carriers, L is the film thickness, and θ is the ratio of the total density of free carriers to the trapped carriers.[18,19] An experimental value of $\alpha \sim 3.5$ was obtained from the *J–E* curves shown in Fig. 6. The deviation is due to the large amount of structural disorders present in the polycrystalline thin films, as discussed above, where the traps do not have a well-defined location causing a broad spreading out of the energy level of the traps and resulting in the observed deviation.[18] SCLC has been a common conduction mechanism in BFO thin films. For instance, Qi *et al.*[10] reported that the trap energy level in the band gap could be created by oxygen vacancies that could activate electrons to be mobile. Hence the high concentration oxygen vacancies in the BFO/SRO 15-min films could well lead to a higher density of charge carriers and hence a deviation from SCLC. Growth conditions can thus strongly affect the structural defects, such as oxygen vacancies in the BFO thin film. For example, the structural inhomogeneities in association with porosity help trap oxygen vacancies and give rise to an enhanced leakage current.

It is well known that bulk BFO is antiferromagnetic and thin-film BFO can exhibit weak ferromagnetism, although the origin of such magnetic behavior is still controversy.[1,20,21] Figure 7 shows the magnetization behavior of the BFO films deposited on SRO-buffered substrates. They all demonstrate a weak saturated ferromagnetic response at room temperature, with a

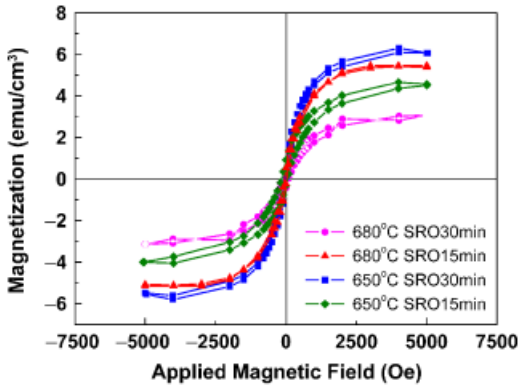

Fig. 7. Magnetization as a function of applied magnetic field for the four BFO films deposited on $SrRuO_3$ (SRO) buffer layers of small grains (SRO 15 min) and large grains (SRO 30 min), thermally annealed at 650° and 680°C, respectively.

saturation magnetization (M_s) ranging between 3.03 and 6.35 emu/cm^3, while the coercivity (H_c) ranging between 23.13 and 111.7 Oe. The annealing temperature and type of substrate buffering did not lead to a largely observable effect on the magnetic behavior. The observation that a larger magnetization in association with a larger leakage current of BFO thin films[4,5] were not shown in the present study. The BFO 650°C/SRO 30-min film, which exhibited the lowest leakage current, also possessed the highest saturation magnetization value among the four BFO films.

IV. Conclusion

The multiferroic behavior of BFO thin films is strongly affected by the morphologies of the SRO buffer layer deposited on Pt/TiO_2/SiO_2/Si substrate. In comparison with a smaller-grained SRO buffer layer, a larger-grained SRO buffer layer is more effective in facilitating the crystallization and growth of a denser BFO perovskite thin film with lesser structural defects, which successfully leads to an enhancement in electrical properties. The BFO 650°C thin films deposited on SRO 30-min buffer layer exhibited a giant polarization ($2P_r$) of 112.5 μC/cm^2 and a coercive field ($2E_c$) of 1045.5 kV/cm. They also demonstrate a desirable fatigue endurance with ~17% degradation upon 10^{10} switching cycles, together the lowest leakage current and the highest saturation magnetization among the BFO films investigated in the present study.

Acknowledgments

The authors acknowledge the support of the National University of Singapore. Dr. Xiaojie Lou committed time and efforts on this manuscript; and his contribution toward this manuscript is acknowledged.

References

[1]J. Wang, J.-B. Neaton, H. Zheng, V. Nagarajan, S.-B. Ogale, B. Liu, D. Viehland, V. Vaithyanathan, D.-G. Schlom, U.-V. Waghmare, N.-A. Spaldin, K.-M. Rabe, M. Wuttig, and R. Ramesh, "Epitaxial $BiFeO_3$ Multiferroic Thin Film Heterostructures," *Science*, **299**, 1719–22 (2003).

[2]Y.-H. Lee, J.-M. Wu, and C.-H. Lai, "Influence of La Doping in Multiferroic Properties of $BiFeO_3$ Thin Films," *Appl. Phys. Lett.*, **88**, 042903 (2006).

[3]R.-Y. Zheng, X.-S. Gao, Z.-H. Zhou, and J. Wang, "Multiferroic $BiFeO_3$ Thin Films Deposited on $SrRuO_3$ Buffer Layer by rf Sputtering," *J. Appl. Phys.*, **101**, 054104 (2007).

[4]S. Geprags, M. Opel, S.-T.-B. Goennenwein, and R. Gross, "Multiferroic Materials Based on Artificial Thin Film Heterostructures," *Philos. Mag. Lett.*, **87**, 141–54 (2007).

[5]W. Eerenstein, F.-D. Morrison, F. Sher, J.-L. Prieto, J.-P. Attfield, J.-F. Scott, and N.-D. Mathur, "Experimental Difficulties and Artefacts in Multiferroic and Magnetoelectric Thin Films of $BiFeO_3$, $Bi_{0.6}Tb_{0.3}La_{0.1}FeO_3$ and $BiMnO_3$," *Philos. Mag. Lett*, **87**, 249–57 (2007).

[6]Fujitsu Microelectronics America Inc., Sunnyvale, CA. http://www.fujitsu.com/ca/en/news/pr/fma_20060802.html, 2006.

[7]Y.-P. Wang, L. Zhou, M.-F. Zhang, X.-Y. Chen, J.-M. Liu, and Z.-G. Liu, "Room-Temperature Saturated Ferroelectric Polarization in $BiFeO_3$ Ceramics Synthesized by Rapid Liquid Phase Sintering," *Appl. Phys. Lett.*, **84**, 1731–3 (2004).

[8]V.-R. Palkar, J. John, and R. Pinto, "Observation of Saturated Polarization and Dielectric Anomaly in Magnetoelectric $BiFeO_3$ Thin Films," *Appl. Phys. Lett.*, **80**, 1628–30 (2002).

[9]W.-M. Zhu and Z.-G. Ye, "Improved Dielectric and Ferroelectric Properties of High Curie Temperature $(1-x)BiFeO_3-xPbTiO_3$ Ceramics by Aliovalent Ionic Substitution," *Appl. Phys. Lett.*, **89**, 232904 (2006).

[10]X. Qi, J. Dho, R. Tomov, M.-G. Blamire, and J.-L.-M. Driscoll, "Greatly Reduced Leakage Current and Conduction Mechanism in Aliovalent-Ion-Doped $BiFeO_3$," *Appl. Phys. Lett.*, **86**, 062903 (2005).

[11]J. Cheng, S. Yu, J. Chen, and Z. Meng, "Dielectric and Magnetic Enhancements in $BiFeO_3$–$PbTiO_3$ Solid Solutions with La Doping," *Appl. Phys. Lett.*, **89**, 122911 (2006).

[12]Y.-H. Lee, J.-M. Wu, Y.-L. Chueh, and L.-J. Chou, "Low-Temperature Growth and Interface Characterization of $BiFeO_3$ Thin Films with Reduced Leakage Current," *Appl. Phys. Lett.*, **87**, 172901 (2005).

[13]G.-W. Pabst, L.-W. Martin, Y.-H. Chu, and R. Ramesh, "Leakage Mechanisms in $BiFeO_3$ Thin Films," *Appl. Phys. Lett.*, **90**, 072902 (2007).

[14]T. Nakamura, Y. Nakao, A. Kamisawa, and H. Takasu, "Preparation of $Pb(Zr,Ti)O_3$ Thin Films on Electrodes Including Ir–O_2," *Appl. Phys. Lett.*, **12**, 1522–4 (1994).

[15]C.-H. Sim, H.-P. Soon, Z.-H. Zhou, and J. Wang, "Fatigue Behavior of Heterostructured $Pb(Zr,Ti)O_3$/$(Bi,Nd)_4Ti_3O_{12}$ Ferroelectric Thin Films," *Appl. Phys. Lett.*, **89**, 122905 (2006).

[16]Y. Wu, M.-J. Forbess, S. Seraji, S.-J. Limmer, T.-P. Chou, and G.-Z. Cao, "Oxygen-Vacancy-Related Dielectric Relaxation in $SrBi_2Ta_{1.8}V_{0.2}O_9$ Ferroelectrics," *J. Appl. Phys.*, **89**, 5647–52 (2001).

[17]Z.-G. Zhu, N.-Z. Zheng, G.-R. Li, and Q.-R. Yin, "Dielectric and Electrical Conductivity Properties of PMS–PZT Ceramics," *J. Am. Ceram. Soc.*, **89**, 717–9 (2006).

[18]H. Hu and S.-B. Krupanidhi, "Current-Voltage Characteristics of Ultrafine-Grained Ferroelectric $Pb(Zr, Ti)O_3$ Thin Films," *J. Mater. Res.*, **9**, 1484–98 (1994).

[19]A. Rose, "Space-Charge-Limited Currents in Solids," *Phys. Rev.*, **97**, 1538–44 (1955).

[20]W. Eerenstein, F.-D. Morrison, J. Dho, M.-G. Blamire, J.-F. Scott, and N.-D. Mathur, "Comment on 'Epitaxial $BiFeO_3$ Multiferroic Thin Film Heterostructures'," *Science*, **307**, 1203a (2005).

[21]J. Wang, A. Scholl, H. Zheng, S.-B. Ogale, D. Viehland, D.-G. Schlom, N.-A. Spaldin, K.-M. Rabe, M. Wuttig, L. Mohaddes, J. Neaton, U. Waghmare, T. Zhao, and R. Ramesh, "Response to Comment on 'Epitaxial $BiFeO_3$ Multiferroic Thin Film Heterostructures'," *Science*, **307**, 1203b (2005). □